Available online at www.sciencedirect.com
SCIENCE DIRECT®
Journal of Solid State Chemistry 178 (2005) 3308–3314
JOURNAL OF SOLID STATE CHEMISTRY
www.elsevier.com/locate/jssc

The crystal chemistry of L-Ta_2O_5 and related structures

I.E. Grey[a,*], W.G. Mumme[a], R.S. Roth[b]

[a]*CSIRO Minerals, Bayview Avenue, Clayton, Vic. 3169, Australia*
[b]*National Institute of Standards and Technology, Gaithersburg, MD, USA*

Received 18 May 2005; received in revised form 15 August 2005; accepted 17 August 2005
Available online 26 September 2005

Abstract

Single crystals of a new form of L-Ta_2O_5 with a $19 \times b$ superstructure have been synthesised by flux growth. The phase is most likely stabilised by the incorporation of a small amount of lithium (0.14 wt% Li) from the flux. The phase has *C*-centred monoclinic symmetry with $a = 6.1939(4)$ Å, $b = 69.549(5)$ Å ($= 19 \times 3.66$ Å), $c = 3.8895(3)$ Å, $\gamma = 90.00(1)^\circ$. The structure was refined in space group $C112/m$ to $R_1 = 0.044$ for 814 unique reflections with $F > 4\sigma(F)$. The structure can be described as comprising chains of edge-shared TaO_7 pentagonal bipyramids that are regularly folded at (010) planes to give sinusoidal chains along [010]. These chains are interconnected along [100] and [001] by corner sharing, creating inter-chain regions that are occupied by isolated TaO_6 octahedra and pairs of corner-shared octahedra. A comparison with published data for high-quality refinements of related structures has led to the development of a general model that can explain the structural chemistry variations in the known L-Ta_2O_5-related structures. A shorthand notation is presented for representing the structures, based on the sequence along [010] of the interchain octahedra.

Keywords: L-Ta_2O_5 structure; 19L Ta_2O_5 superstructure; Crystal chemistry of L-Ta_2O_5-related phases

1. Introduction

Tantalum oxide, Ta_2O_5, and ternary phases containing Ta_2O_5 are currently of considerable interest as efficient photocatalysts for decomposition of organics and for splitting water to form hydrogen [1,2]. For different structural polymorphs of the same composition, the photocatalytic activity has been found to be structure dependent [3]. It is thus important to have good structural characterisation of different polymorphs in order to help understand the influence of structure on photoactivity.

The structural characterisation of Ta_2O_5 has continued to pose challenges to crystallographers for more than 50 years since Lagergren and Magneli [4] reported that Ta_2O_5 undergoes a low-to-high temperature structure transformation at ~1320 °C. In particular, the low temperature form, L-Ta_2O_5 has proved difficult to characterise structurally. Lehovec [5] analysed powder X-ray diffraction data to obtain the substructure of L-Ta_2O_5 in an orthorhombic cell with $a = 6.20$ Å, $b = 3.66$ Å, $c = 3.89$ Å. He reported the presence of many weak superstructure lines and presented unit cells from previous literature studies that corresponded to superstructures along [010] with multiplicities (m) of $12 \times b$ and $19 \times b$. Lehovec [5] made the important observation that a low density of packing of oxygen atoms in (010) planes at $z = 0.5$ should readily enable the incorporation of interstitial cations in these planes (as was subsequently found in the related T-Nb_2O_5 structure [6]).

A limitation common to the early studies on L-Ta_2O_5 was that only powder specimens could be prepared for analysis. This situation changed when Roth and Waring [7] showed that addition of oxides such as WO_3 helped to stabilise L-Ta_2O_5 related structures in phases that had congruent melting points so that single crystals could be grown from the melt. Stephenson and Roth [8–10] subsequently published a series of papers in which they reported single crystal structure determinations for $Ta_{22}W_4O_{67}$, $Ta_{30}W_2O_{81}$ and $Ta_{38}WO_{98}$, with *b*-axis

*Corresponding author. Fax: +61 3 9562 8919.
E-mail address: ian.grey@csiro.au (I.E. Grey).

0022-4596/$ - see front matter Crown Copyright © 2005 Published by Elsevier Inc. All rights reserved.
doi:10.1016/j.jssc.2005.08.011

multiplicities, $m = 13, 8$ and 19, respectively. They also succeeded in growing small crystals of L-Ta_2O_5 with $m = 11$ and determined its structure [11].

On the basis of the single crystal structure determinations, Roth and Stephenson [12] developed a structural model which systematised the relations between the ideal, undistorted structures and allowed the prediction of intermediate structures. The model involved the periodic folding, or twinning, of edge-shared chains of MO_7 pentagonal bipyramids to give sinusoidal chains along [010] that were connected together along [100] and [010] by corner sharing. This type of linkage gave rise to two types of inter-chain regions, containing either one metal atom (in straight-chain sections) or pairs of metal atoms (at the folded regions). These inter-chain metals had octahedral coordination in the ideal structures. The features of the model are illustrated in Fig. 1.

Roth and Stephenson's [12] model comprised a set of basic structures, containing an even number, n, of MO_7 units per chain length, with $n \geqslant 4$. The corresponding b-axis periodicities were related to n by $m = 3n/2 - 1$, giving $m = 5, 8, 11, 14$, etc. An infinite number of intermediate structures (such as their $m = 13$ and 19 structures) could be constructed by intergrowth of the basic structures. In practise, the L-Ta_2O_5 phase field was found to comprise superstructures with b-axis multiplicities in the range $m = 11$ (high temperature limit) to $m = 14$ (stable low temperature structure). The compositions of the phases obtained from the structure analyses were found to have lower metal: oxygen ratios than the prepared materials. Roth and Stephenson [12] proposed that the correct stoichiometry was achieved by having oxygen vacancies in so-called (010) distortion planes in the vicinity of the folded regions of the chains.

In the 1990s, Schmid and colleagues published a comprehensive series of papers on the structures of L-Ta_2O_5 related phases in the WO_3–Ta_2O_5 system [13–16]. They treated the compositions $(1-x)Ta_2O_5 \cdot xWO_3$, $0 \leqslant x \leqslant 0.267$, as a composite modulated solid solution

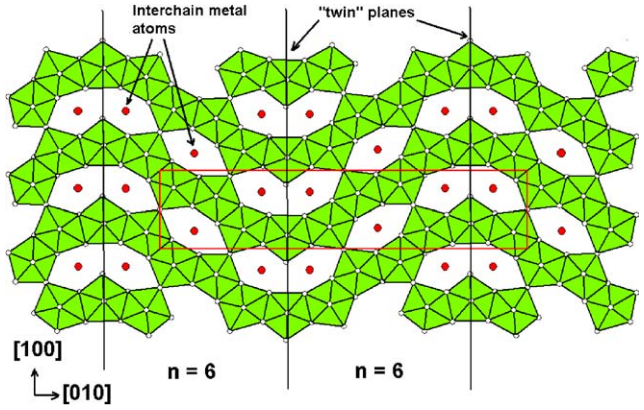

Fig. 1. Roth and Stephenson [12] model for L-Ta_2O_5-related structures, viewed in projection along [001]. Filled circles correspond to metal atom sites located between the sinusoidal chains of edge-shared pentagonal bipyramids. Vertical lines indicate where the chains are folded.

and analysed the structures using a superspace approach. Their refinements showed that the complete composition region can be represented structurally by the same set of periodic atomic modulation functions. For two compositions, $Ta_{22}W_4O_{67}$ ($m = 13$) and $Ta_{74}W_6O_{203}$ ($m = 8$) Schmid et al. [13] conducted conventional commensurate superstructure refinements, in space groups $C112/m$ and $Pbam$, respectively. The distribution of pentagonal bipyramids and octahedra in their models for both structures differed from those reported by Roth and Stephenson [12]. In order to match the structure-derived compositions to the chemical compositions, Schmid et al. [13] proposed that oxygen vacancies were distributed over apical oxygen positions at $z = 0.5$, whereas Roth and Stephenson [12] had the oxygen vacancies located at $z = 0$.

In contrast to the models presented by Roth and Stephenson [12] and by Schmid et al. [13], Marinder [17,18] presented an alternative description of L-Ta_2O_5 related structures in terms of intergrowths of α-U_3O_8 and β-U_3O_8 type elements, where the β-U_3O_8 segments correspond to the straight-chain sections in Fig. 1 and the α-U_3O_8 segments correspond to the folded chain segments. Marinder [17] commented that the role of interstitial atoms in achieving stoichiometry as in T-Nb_2O_5 may be common to L-Ta_2O_5 related structures.

In view of the inconsistencies in the different models for L-Ta_2O_5 presented above, we initiated a study which centred on the successful flux growth of the $m = 19$ modification of L-$Ta_2O_5 \equiv$ 19L-Ta_2O_5. In this paper, the results obtained from the single crystal refinement of 19L-Ta_2O_5 are combined with the high quality structure refinements for the $m = 8$ and 13 phases reported by Schmid et al. [13] to develop a consistent description of the L-Ta_2O_5 related phases.

2. Experimental

Crystals of 19L-Ta_2O_5 were grown from a lithium molybdate flux of composition $Li_4Mo_5O_{17}$. A mixture of Ta_2O_5 powder and flux in the weight ratio 80:20 was contained in an open platinum crucible and heated at 1200 °C until most of the flux was evaporated. The product was washed in hot water to leach the flux, leaving green coloured hexagonal crystals. The crystals were heated for 4 h at 1600 °C to drive off any residual flux, resulting in the colour of the crystals changing to a light straw colour. Analyses of the heated crystals for flux elements (ICP-AAS for Li, electron microprobe analyses for Mo) gave residual levels of 0.14 wt% Li and 0.05 wt% Mo. Analysis of the green crystals gave 0.06–0.14 wt% Mo.

Precession photographs gave similar diffraction patterns for both flux-prepared green crystals and the subsequently heated straw crystals, although the diffraction spots in the patterns for the green crystals were somewhat more diffuse compared to the very sharp spots in the patterns for the heated crystals. The precession photographs showed apparent C-centred orthorhombic symmetry with

$a = 6.20$ Å, $b = 69.5$ Å, $c = 3.88$ Å. However subsequently collected diffractometer intensity data showed that the true symmetry was *C*-centred monoclinic. The *b*-axis dimension of 69.5 Å is equal to 19×3.66 Å, confirming $m = 19$. A small lath-shaped straw-coloured crystal was used for an intensity data collection using a Nonius Kappa CCD diffractometer. The data collection parameters are given in Table 1. The intensity data set was processed to produce an absorption-corrected data set, which was used with SHELXL [19] for the structure analysis. The merge statistics were consistent with a diffraction symmetry of $112/m$.

Initially the Stephenson and Roth [10] $m = 19$ model for $Ta_{38}WO_{98}$ was used in a structure refinement. We were unable to obtain a satisfactory refinement of this model, as might be expected because of its lack of adherence to the experimentally observed *C*-centering. The model was then modified to change the sequence of edge-shared chains of TaO_7 from 6–6–8–8 to 6–8–6–8, as suggested by Harburn et al. [20] from a transmission electron microscopy study of a $m = 19$ structure in the Ta_2O_5–TiO_2 system. Refinement of this model in $C112/m$ converged to $R_1 = 0.07$.

At this point a difference Fourier map showed significant electron density in a number of sites located at the level of the apical oxygen atoms at $z = 0.5$. These were identified as tri-capped trigonal prismatic sites, analogous to those reported in T-Nb_2O_5 [6]. Incorporation of tantalum atoms at these sites and refinement of their site occupancies resulted in convergence at $R_1 = 0.044$ for 814 reflections with $F > 4\sigma(F)$. Anisotropic temperature factors were used for the normal site Ta atoms only. The inclusion of the interstitial atoms gave a calculated unit cell composition from the structure refinement of $Ta_{39.73}O_{100}$. The remaining small shortfall in positive charge (a deficiency of +1.35 charges per unit cell) is most likely met by lithium ion incorporation from the flux used for the crystal growth. The chemically analysed content of 0.14 wt% Li corresponds to 1.8 Li^+ per unit cell.

Further refinement details are given in Table 1. A list of refined coordinates and isotropic atomic displacement parameters are reported in Table 2. Anisotropic atomic displacement parameters for the normal-site metal atoms can be obtained from the authors.

Table 1
Data collection conditions and refinement parameters for 19L-Ta_2O_5

Crystal data	
Unit cell composition	$Ta_{39.73}Li_{1.35}O_{100}$
Cell parameters	$a = 6.1939(4)$ Å
	$b = 69.549(5)$ Å
	$c = 3.8895(3)$ Å
	$\gamma = 90.00(1)^\circ$
Space group	$C112/m$
Calculated density	8.72 g/cm^3
Data collect	
Temperature (K)	295
λ (Mo$K\alpha$)	0.71073
Crystal size (mm)	$0.08 \times 0.08 \times 0.02$
Collection mode	ϕ-scan $0-360^\circ + 2\Omega$ scans, 0.5° steps
Count time per frame	15 s
2θ max	55°
Data completeness	97.6%
Reflection range	$-8 \leqslant h \leqslant 8$, $k \leqslant 49$, $1 \leqslant 5$
Total no. of reflections	5692
No. of unique reflections	1337
No. of reflections, $F > 4\sigma(F)$	814
Absorption correction	Analytical, face indexing, $\mu = 65.2$ mm^{-1}
	$T_{min} = 0.020$, $T_{max} = 0.283$
R(merge)	0.04
Refinement	
No. of parameters refined	157
R_1, $F > 4\sigma(F)$	0.044
R_1, all data	0.089
wR_2 (F^2), all data	0.14
GOF	0.92

3. Results and discussion

3.1. The 19L-Ta_2O_5 structure

A polyhedral representation of the 19L-Ta_2O_5 structure, viewed in projection along [001] is shown in Fig. 2. Assignments of Ta atoms to octahedral and pentagonal bipyramidal sites were made with reference to the ranges of Ta–O bond lengths given in Table 3. As this table shows, the assignment of the four inter-chain sites, Ta(1)–Ta(4), to octahedral coordination is unambiguous, as each site has six Ta–O distances in a relatively narrow range, 1.89–2.04 Å and the next nearest oxygen atom is at least 2.85 Å away. The seventh Ta–O distance is thus comparable to second-nearest-neighbour distances between normal site and interstitial site Ta atoms (e.g. Ta(1)–Ta(i1) = 2.87(1) Å). Likewise, the assignment of pentagonal bipyramidal coordination to atoms Ta(5)–Ta(9) is unambiguous as they all have seven Ta–O distances in the range 1.94–2.38 Å. The only 'transition'' coordination is for Ta(10), which has six Ta–O distances in the range 1.94–2.07 Å and a seventh distance Ta(10)–O(15) at 2.55(2) Å. If this site is considered as a distorted pentagonal bipyramidal site then the sites Ta(5)–Ta(10) form the folded chains of edge-shared pentagonal bipyramids shown in Fig. 2.

The oxygen atom O(15) involved in the transition distance of 2.55 Å, is located in the folded-chain region and is bonded to two pentagonal bipyramids and one octahedron as illustrated in Fig. 2. It corresponds to an oxygen vacancy site in the Roth and Stephenson [12] model (see their Fig. 9). Refinement of the better quality diffraction data used in this study shows that such vacant sites do not occur. An almost identical situation pertains to the refined $m = 13$ structure for $Ta_{22}W_4O_{67}$ [13], where the site M(6) in the folded chain region has six M–O distances of 1.99–2.08 Å and a seventh distance, M(6)–O(9) = 2.57 Å. In this case O(9) would correspond

Table 2
Refined coordinates and isotropic displacement parameters for 19L-Ta_2O_5

Atom	x	y	z	U (Å^2)
Ta1	0.4752(2)	0.86660(3)	0	0.0169(6)
Ta2	0.4731(2)	0.92219(3)	0	0.0214(7)
Ta3	0.9835(2)	0.78908(3)	0	0.0137(6)
Ta4	0	0	0	0.0195(8)
Ta5	0.9179(2)	0.89520(3)	0	0.0137(6)
Ta6	0.4308(2)	0.81472(3)	0	0.0140(6)
Ta7	0.4511(2)	0.97513(3)	0	0.0164(6)
Ta8	0.0022(2)	0.94516(3)	0	0.0200(6)
Ta9	0.5247(2)	0.76499(3)	0	0.0205(6)
Ta10	0.9859(2)	0.84435(3)	0	0.0169(6)
Ta1i	0.282(2)	0.8918(3)	0.5	0.030(6)
Ta2i	0.801(2)	0.9707(3)	0.5	0.033(6)
Ta3i	0.791(2)	0.8196(2)	0.5	0.028(4)
Ta4i	0.322(4)	0.7393(5)	0.5	0.03(1)
Ta5i	0.660(10)	0.9490(12)	0.5	0.06(3)
Ta6i	0.650(12)	0.8360(14)	0.5	0.02(3)
O1	0.697(3)	0.8308(4)	0	0.022(6)
O2	0.563(3)	0.8948(3)	0	0.011(5)
O3	0.335(3)	0.9475(4)	0	0.017(7)
O4	0.686(4)	0.9930(4)	0	0.030(7)
O5	0.079(3)	0.8170(4)	0	0.019(6)
O6	0.802(3)	0.9221(3)	0	0.005(4)
O7	0.099(3)	0.9743(4)	0	0.024(6)
O8	0.861(3)	0.7642(4)	0	0.021(6)
O9	0.306(3)	0.7866(3)	0	0.009(5)
O10	0.320(4)	0.8425(4)	0	0.030(7)
O11	0.170(3)	0.9161(3)	0	0.011(5)
O12	0.804(3)	0.8680(3)	0	0.013(5)
O13	0.924(3)	0.8940(4)	0.5	0.020(6)
O14	0.525(3)	0.7659(4)	0.5	0.021(6)
O15	0.170(3)	0.8772(3)	0	0.021(6)
O16	0.717(4)	0.9583(4)	0	0.034(7)
O17	0.25	0.75	0	0.028(9)
O18	0.675(3)	0.7949(3)	0	0.015(5)
O19	0.992(3)	0.8449(3)	0.5	0.011(5)
O20	0.491(3)	0.8656(4)	0.5	0.018(6)
O21	0.010(3)	0.9441(4)	0.5	0.017(6)
O22	0	0	0.5	0.040(11)
O23	0.436(3)	0.8153(4)	0.5	0.023(6)
O24	0.996(3)	0.7883(4)	0.5	0.030(7)
O25	0.454(3)	0.9757(4)	0.5	0.017(5)
O26	0.486(3)	0.9231(4)	0.5	0.036(8)

Refined site occupation factors of interstitial sites Ta1i–Ta6i are 0.052(3), 0.050(3), 0.061(3), 0.028(3), 0.016(3) and 0.009(3), respectively.

Table 3
List of Ta–O distances (<3.4 Å) in19L-Ta_2O_5

Ta–O	Distance (Å)	Ta–O	Distance (Å)
Normal site Ta atoms			
Ta(1)–O(10)	1.94(2)	Ta(6)–O(23) × 2	1.941(5)
–O(20) × 2	1.944(5)	–O(1)	1.99(2)
–O(15)	2.03(2)	–O(18)	2.05(2)
–O(2)	2.03(2)	–O(10)	2.05(3)
–O(12)	2.04(2)	–O(9)	2.10(2)
–O(1)	2.85(2)	–O(5)	2.19(2)
Ta(2)–O(11)	1.93(2)	Ta(7)–O(4)	1.91(2)
–O(26) × 2	1.943(5)	–O(25) × 2	1.940(5)
–O(2)	1.98(2)	–O(16)	2.02(2)
–O(3)	1.96(3)	–O(3)	2.05(2)
–O(6)	2.04(2)	–O(7)	2.18(2)
–O(16)	2.95(2)	–O(4)	2.37(3)
Ta(3)–O(8)	1.89(2)	Ta(8)–O(21) × 2	1.942(5)
–O(24) × 2	1.942(5)	–O(16)	1.99(2)
–O(18)	1.96(2)	–O(6)	2.03(2)
–O(9)	2.01(2)	–O(3)	2.07(2)
–O(5)	2.03(2)	–O(7)	2.11(2)
–O(17)	3.18(2)	–O(11)	2.27(2)
Ta(4)–O(7) × 2	1.89(3)	Ta(9)–O(14) × 2	1.941(5)
–O(22) × 2	1.940(5)	–O(17)	1.997(3)
–O(4) × 2	2.01(2)	–O(9)	2.02(2)
–O(16)	3.39(2)	–O(8)	2.08(2)
		–O(8)	2.15(3)
		–O(18)	2.28(2)
Ta(5)–O(13) × 2	1.942(5)	Ta(10)–O(19) × 2	1.941(5)
–O(6)	2.00(2)	–O(12)	1.99(2)
–O(15)	2.00(2)	–O(5)	1.99(3)
–O(12)	2.02(2)	–O(1)	2.03(2)
–O(11)	2.13(2)	–O(10)	2.08(2)
–O(2)	2.20(2)	–O(15)	2.55(2)
Interstitial Ta atoms	*Range of 9 Ta(i)–O*		
Ta(1i)	2.22–2.67	Ta(4i)	2.12–2.77
Ta(2i)	2.18–2.69	Ta(5i)	2.10–2.83
Ta(3i)	2.16–2.69	Ta(6i)	1.95–3.10

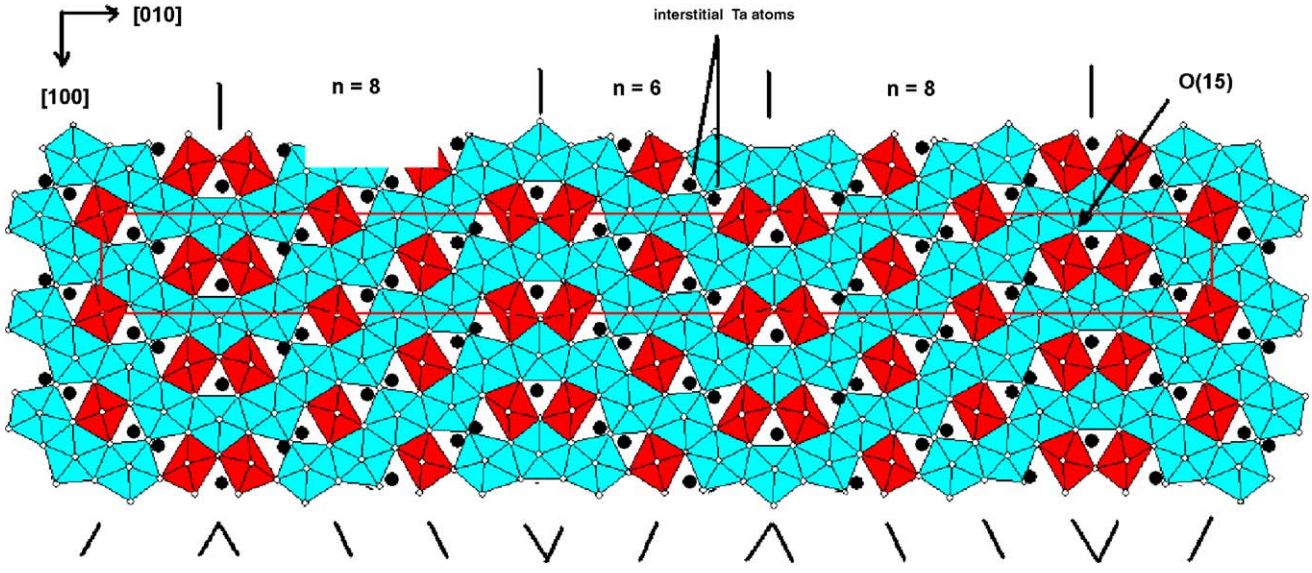

Fig. 2. Polyhedral representation of the structure for 19L-Ta_2O_5 in projection along [001]. TaO_6 octahedra are dark-shaded and TaO_7 pentagonal bipyramids are light shaded. The shaded circles correspond to interstitial Ta atoms. The number of TaO_7 polyhedra per chain length, 8–6–8–6, is shown. The shorthand symbols for the sequence of octahedral sites along [010], shown schematically along the bottom, matches with the data in Table 4. The marked anion, O(15) is referred to in the text.

to Roth and Stephenson's vacant anion site but in the excellent refinement obtained by Schmid et al. [13], O(9) has normal atomic displacement parameters.

The structural model for 19L-Ta_2O_5, considering normal Ta sites only, gives a unit cell content of $Ta_{38}O_{100}$, whereas stoichiometry requires $Ta_{40}O_{100}$. The refinement confirmed that the stoichiometry is achieved predominantly by interstitial Ta atoms. These are shown by the filled circles in Fig. 2. The interstitial Ta atoms are 9-coordinated to oxygen in the form of tri-capped trigonal prisms. Such 9-coordinated interstitial metal atom sites have been reported in the structurally related T-Nb_2O_5 [6] and also in the tetragonal tungsten bronze-type structure for $K_6Ta_{10.8}O_{30}$ [21]. Refinement of the site occupancies of the interstitial Ta atoms in 19L-Ta_2O_5 gave an additional 1.73 atoms per unit cell, bringing the composition close to stoichiometry. The shortfall of 1.35 positive charges is probably met by lithium incorporation. 1.35 Li atoms per unit cell corresponds to 0.11 wt% Li, which is close to the chemically analysed value of 0.14% Li. The presence of lithium also provides an explanation for the stability of the L-Ta_2O_5 phase when it was heated at 1600°C, which is above the low-to-high transformation temperature for pure Ta_2O_5 [22].

The polyhedral model for 19L-Ta_2O_5 shown in Fig. 2 adheres to the general model proposed by Roth and Stephenson [12] for ideal L-Ta_2O_5 related structures, in comprising folded chains of edge-shared pentagonal bipyramids, with octahedra occupying the inter-chain regions. However there are two important differences of detail when the refined 19L-Ta_2O_5 structure is compared with Roth and Stephenson's [12] structure for $m = 19$ $Ta_{38}WO_{98}$. The number of TaO_7 in successive chain segments is in the sequence 6–8–6–8 rather than 6–6–8–8 as reported by Roth and Stephenson [12], and the stoichiometry is achieved with Ta interstitial atoms rather than with oxygen vacancies. Anion distortion sheets do not occur in 19L-Ta_2O_5 and the general polyhedral distortions are much closer to those in Roth and Stephenson's ideal polyhedral models than to their real models obtained from refinement.

3.2. Comparison with $m = 8$ and 13 structures

Schmid et al.'s [13] refined $m = 13$ structure for $Ta_{22}W_4O_{67}$ has closely similar structural features to those for 19L-Ta_2O_5. In particular, in $Ta_{22}W_4O_{67}$ the inter-chain octahedra have almost identical M–O ranges to those in 19L-Ta_2O_5 (6 M–O in the range 1.91–2.03 Å and the seventh M–O distance at >2.9 Å). The pentagonal bipyramid sites also have similar M–O ranges to those reported above for 19L-Ta_2O_5 (three sites have seven M–O in the range 1.93–2.33 Å, while the fourth site has 6 M–O in the range 1.91–2.08 Å and a seventh "transition" distance at 2.57 Å). A polyhedral representation of the refined structure for $Ta_{22}W_4O_{67}$ is shown in Fig. 3. In this case the

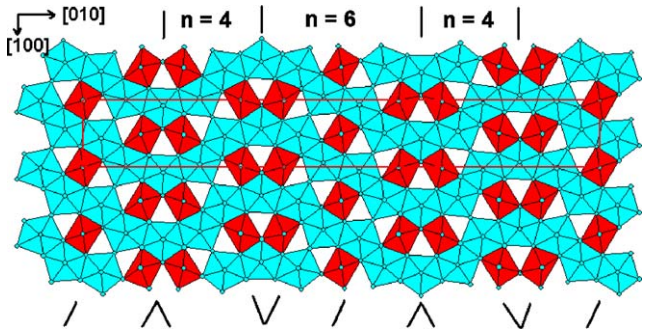

Fig. 3. The [001] projection of the $m = 13$ structure for $Ta_{22}W_4O_{67}$, from Ref. [13]. Same labelling as in Fig. 2.

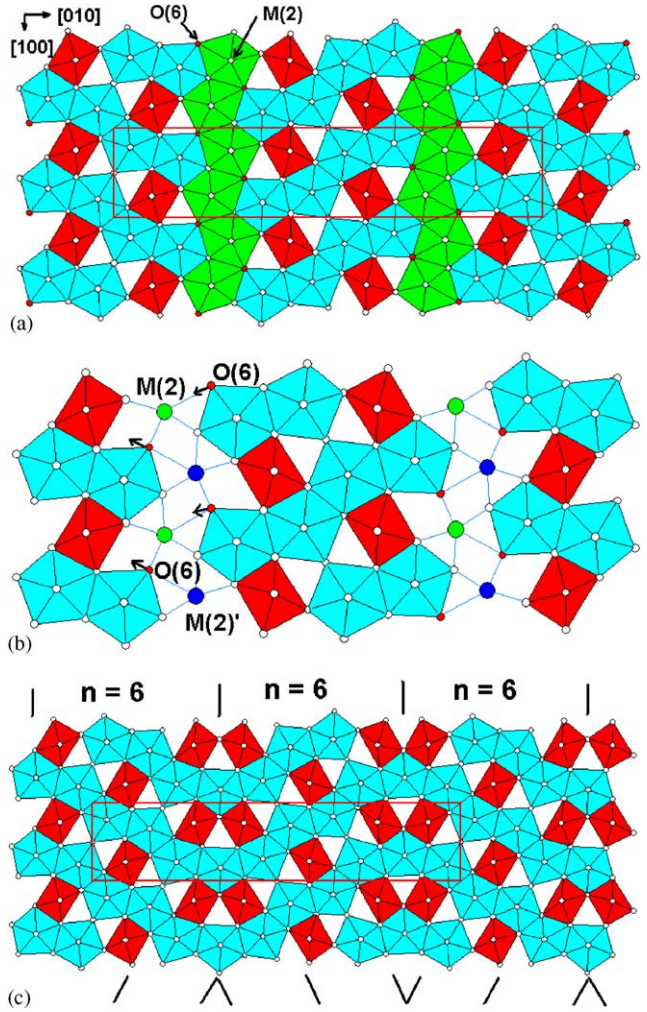

Fig. 4. (a) [001] projection of the $m = 8$ structure for $Ta_{74}W_6O_{203}$, space group *Pbam*, from Schmid et al. [13]. The medium-grey shaded vertical columns of edge shared MO_7 polyhedra are not consistent with the polyhedral models for the $m = 19$ and 13 structures shown in Figs. 2 and 3. The labelled atom sites O(6) and M(2) are referred to in the text. (b) The arrows show the movements of O(6), in space group $Pb2_1m$, which convert two distorted $M(2)O_7$ polyhedra to a regular $M(2)O_7$ pentagonal bipyramid and a $M(2)'O_6$ octahedron. (c) Representation of the $m = 8$ structure in space group $Pb2_1m$.

Table 4
Structural systematics in L-Ta_2O_5 related structures

N	M	Sequence of octahedra	Symmetry	Examples	Ref.
4	5	/\\/	P	$U_5O_{12}Cl$	[23]
4+6	13	/\\/ /\\/	C	$Ta_{22}W_4O_{67}$	[13]
6	8	/\\\/	P	T-Nb_2O_5	[6]
				$Ta_{30}W_2O_{81}$	[9]
6+8	19	/\\\\/ /\\\\/	C	L-Ta_2O_5	This work
				$Ta_{38}WO_{98}$	[10]
8	11	//\\\/	P	L-Ta_2O_5	[11]
10	14	///\\\\/	P	$Ta_{54}Zr_2O_{139}$	[12]
				L-Ta_2O_5	[24]

number of edge-shared MO_7 pentagonal bipyramids in successive chain segments is in the sequence 4–6–4–6.

A problem arises in the case of the refined $m = 8$ structure for $Ta_{74}W_6O_{203}$ [13]. An [001] projection of the structure refined in *Pbam* is shown in Fig. 4(a). It is clearly not consistent with the representations of the $m = 19$ and 13 structures shown in Figs. 2 and 3. In $Ta_{74}W_6O_{203}$ the edge-shared pentagonal bipyramids form columns along [100] as well as sinusoidal chains along [010], and so the structure can no longer be described in terms of corner linking of folded chains of MO_7 polyhedra. The [100] columns of M(2)–O_7 polyhedra are unusual in that one distance, M(2)–O(6) = 2.68 Å, is significantly more transitional than found in the other two structures, making the coordination more ambiguous.

An inspection of the published [13] anisotropic displacement parameters for $Ta_{74}W_6O_{203}$ shows that O(6) has the highest U_{ii} values of all the oxygen atoms, corresponding to a mean square displacement of ~0.2 Å, with the major displacement component along [010]. This suggests a possible solution to the dilemma. $Pb2_1m$ is an alternative possible space group for $Ta_{74}W_6O_{203}$ based on superspace-group symmetry [15], and in $Pb2_1m$, O(6) can be split into two independent sites. Displacement of the two different O(6) sites by ~0.2 Å approximately along [010] as shown in Fig. 4(b), changes the coordination of the M(2) site from two very distorted M(2)O_7 polyhedra to a less distorted M(2)O_7 site plus an octahedral M(2)′O_6 site, with M–O distances comparable to those in the $m = 13$ and 19 structures. The resulting $Pb2_1m$ description of the $m = 8$ structure is shown in polyhedral form in Fig. 4(c). The close relationship with the $m = 19$ and 13 structures shown in Figs. 2 and 3 is obvious.

3.3. A shorthand description of L-Ta_2O_5 structures

Considering only the inter-chain octahedral positions in 19L-Ta_2O_5, the sequence of single octahedra and pairs of octahedra as shown in Fig. 2 can be represented schematically by

/\\\\/ /\\\\/

where the / or \ and /\ or \/ indicate the orientations of the isolated octahedra and the corner-connected pairs of octahedra as shown on Figs. 2, 3 and 4(c), and the vertical offset represents the *C*-centering displacements. The corresponding schematic for the primitive cell $m = 8$ structure from Fig. 4(c) is

/\\\/

This approach is a convenient shorthand way to represent these structures and it has been extended to the range of known L-Ta_2O_5-related structures in Table 4.

4. Conclusions

- The Roth and Stephenson [12] model gives a consistent description of L-Ta_2O_5 related phases if *maximum alternation* of chain lengths is considered for intergrowths of different chain lengths. The model comprises periodically folded chains of edge-shared pentagonal bipyramids directed along [010] which are inter-connected along [100] and [001] via corner sharing, forming regions occupied by single or pairs of octahedrally coordinated metal atoms.
- The published $m = 8$ structure for $Ta_{74}W_6O_{203}$ [13] is not consistent with the above model. It can be made consistent by a lowering of the space group symmetry from *Pbam* to $Pb2_1m$, allowing splitting of two strongly distorted MO_7 sites to a regular MO_7 site plus a MO_6 octahedral site.
- Stoichiometry in 19L-Ta_2O_5, as in T-Nb_2O_5 [6] is achieved through M atom interstitials. The interstitial metal atoms are 9-coordinated, in the form of tri-capped trigonal prisms. This contrasts with the ternary L-$(Ta,W)_2O_5$ phases for which oxygen vacancies have been proposed to achieve stoichiometry [12,13].
- The range of L-Ta_2O_5 related structures can be conveniently represented by a shorthand notation giving the sequence of single octahedra and pairs of octahedra, including an offset of the symbols to indicate *C*-centred cells.

- The 19L-Ta_2O_5 phase is strictly not a binary phase. It has an analysed content of 0.14 wt% Li that is derived from the flux used for crystal growth. The contained lithium most likely explains the stability of the low temperature form at 1600 °C.

Acknowledgments

We thank Cheryl McHugh for the ICP-AAS analyses, Colin MacRae for the electron microprobe analyses and Gary Fallon for the X-ray intensity data collection. Thanks also to an anonymous referee who pointed out the likely role of Li in stabilising L-Ta_2O_5 at 1600 °C.

References

[1] Y. Zhu, F. Yu, Y. Man, Q. Tian, Y. He, N. Wu, J. Solid State Chem. 178 (2005) 224–229.
[2] Z. Zou, H. Arakawa, J. Photochem. Photobiol. A 158 (2003) 145–162.
[3] H. Kato, A. Kudo, Catal. Today 78 (2003) 561–569.
[4] S. Lagergren, A. Magneli, Acta Chem. Scand. 6 (1952) 444–446.
[5] K. Lehovec, J. Less-Common Met. 7 (1964) 397–410.
[6] K. Kato, S. Tamura, Acta Crystallogr. B 31 (1975) 673–677.
[7] R.S. Roth, J.L. Waring, J. Res. Natl. Bur. Stand. 74A (1970) 485–493.
[8] N.C. Stephenson, R.S. Roth, Acta Crystallogr. B 27 (1971) 1010–1017.
[9] N.C. Stephenson, R.S. Roth, Acta Crystallogr. B 27 (1971) 1018–1024.
[10] N.C. Stephenson, R.S. Roth, Acta Crystallogr. B 27 (1971) 1031–1036.
[11] N.C. Stephenson, R.S. Roth, Acta Crystallogr. B 27 (1971) 1037–1044.
[12] R.S. Roth, N.C. Stephenson, in: L. Eyring, M. O'Keeffe (Eds.), The Chemistry of Extended Defects in Non-Metallic Solids, North-Holland, Amsterdam, 1970, pp. 167–181.
[13] S. Schmid, J.G. Thompson, A.D. Rae, B.D. Butler, R.L. Withers, N. Ishizawa, S. Kishimoto, Acta Crystallogr. B 51 (1995) 698–708.
[14] S. Schmid, R.L. Withers, J.G. Thompson, J. Solid State Chem. 99 (1992) 226–242.
[15] A.D. Rae, S. Schmid, J.G. Thompson, R.L. Withers, N. Ishizawa, Acta Crystallogr. B 51 (1995) 709–721.
[16] S. Schmid, K. Futterer, J.G. Thompson, Acta Crystallogr. B 52 (1996) 223–231.
[17] B.-O. Marinder, Acta Chem. Scand. 44 (1990) 123–134.
[18] B.-O. Marinder, J. Solid State Chem. 160 (2001) 62–68.
[19] G.M. Sheldrick, SHELX93, Program for the Refinement of Crystal Structures, University of Gottingen, 1993.
[20] G. Harburn, R.J.D. Tilley, J.M. Williams, R.P. Williams, J. Hutchison, J. Chem. Soc. Faraday Trans. 88 (1992) 621–624.
[21] A.A. Awadalla, B.M. Gatehouse, J. Solid State Chem. 23 (1978) 349–355.
[22] R.S. Roth, H.S. Parker, W.S. Brower, J.L. Waring, in: W. Van Gool, (Ed.), Fast Ion Transportation of Solids, Solid State Battery Devices, Proceedings of the NATO Advanced Study Institute, Belgirate, Italy, 1972, North-Holland, Amsterdam, 1973, pp. 217–232.
[23] E.H.P. Cordfunke, P. van Vlaanderen, K. Goubitz, B.O. Loopstra, J. Solid State Chem. 56 (1985) 166.
[24] C. Askeljung, B.-O. Marinder, M. Sundberg, J. Solid State Chem. 176 (2003) 250–258.